Zinc ferrite nanoparticles as MRI contrast agents†

Carlos Bárcena,[a] Amandeep K. Sra,[a] Girija S. Chaubey,[b] Chalermchai Khemtong,[a] J. Ping Liu[b] and Jinming Gao*[a]

Received (in Cambridge, UK) 21st January 2008, Accepted 15th February 2008
First published as an Advance Article on the web 11th March 2008
DOI: 10.1039/b801041b

Mixed spinel hydrophobic $Zn_xFe_{1-x}O{\cdot}Fe_2O_3$ (up to $x = 0.34$) nanoparticles encapsulated in polymeric micelles exhibited increased T_2 relaxivity and sensitivity of detection over clinically used Feridex®.

Magnetic resonance imaging (MRI) is a powerful clinical imaging technique for the non-invasive diagnosis and post-therapy assessment of a variety of diseases. MRI contrast can be enhanced by the use of positive or negative contrast agents resulting in brighter (T_1-weighted) or darker (T_2-weighted) images, respectively. Superparamagnetic iron oxide (SPIO)[1–4] nanoparticles are T_2 contrast agents that are widely used in molecular and cellular imaging applications. While most of the work in this area has been focused on acquiring biological specificity of SPIO by surface modifications,[2,3] it still remains an open challenge to improve the magnetic properties of SPIO which would, in turn, lead to higher imaging sensitivity.

Recently, a series of spinel-structured ferrites, MFe_2O_4 ($M = Mn^{2+}$, Fe^{2+}, Co^{2+}, Ni^{2+}), were reported as novel MRI contrast agents.[5] In the spinel structure of general formula AB_2O_4 there are twice as many octahedral (B) sites as tetrahedral (A) sites. If M^{2+} occupies only the A sites, the spinel is normal; if it occupies only the B sites, the spinel is inverse. In the above series, $MnFe_2O_4$ has a mixed spinel structure (*i.e.*, Mn^{2+} occupies both A and B sites), whereas the other metal ferrites have an inverse spinel structure.[5,6] When an external magnetic field is applied, the magnetic spins at B sites align in parallel with the direction of the external magnetic field, but those at A sites align antiparallel. Since the number of B sites is twice that of the A sites, a non-compensated magnetic moment occurs due to the dominant A–B interactions.

In contrast to the above MFe_2O_4, $ZnFe_2O_4$ has a normal spinel structure with the A sites preferentially occupied by the Zn^{2+} ions, which renders antiferromagnetic properties and makes it a poor choice for MRI applications. However, it has been demonstrated in bulk materials that addition of $ZnFe_2O_4$ into an inverse spinel structure (*e.g.*, Fe_3O_4) can significantly increase the net magnetic moment of the resulting mixed spinel structure.[6–10] In the present work, we demonstrate a novel controlled synthesis of non-stoichiometric zinc ferrite nanoparticles, $Zn_xFe_{1-x}O{\cdot}Fe_2O_3$ (also abbreviated as Zn-SPIO) and their potential application as a highly sensitive MRI contrast agent. Compared to Mn-ferrites,[5] one potential key advantage of Zn-SPIO nanoparticles is the reduced toxicity of Zn over Mn. For example, the Food and Drug Administration has set the reference daily intake (RDI) doses for Fe and Zn at 18 and 15 mg/day, respectively, which is much higher than the Mn value (2 mg/day).[11]

As a proof of concept, we chose 4–5 nm Zn-SPIO nanoparticles as a model system. The use of similar sized nanoparticles eliminates the experimental artifacts that may arise from the size dependence of the contrast agent. Zn-SPIO synthesis was achieved through modification of a published procedure on metal ferrites.[12] One of the major challenges in Zn-SPIO synthesis is the difficulty in incorporating electropositive Zn^{2+} into the spinel structure with simultaneous control of stoichiometry and size. Our initial attempts using $Zn(acac)_2$ resulted in polydispersed samples with no control over stoichiometry and size. Thus, we modified our synthetic strategy and used diethyl zinc (Et_2Zn) with iron acetylacetonate ($Fe(acac)_3$) during synthesis. In a typical reaction, $Fe(acac)_3$, 1,2-hexadecanediol, oleic acid, octyl ether–diphenyl ether and hexadecylamine (HDA) were heated to 150 °C under argon. Controlled amounts of Et_2Zn were then hot-injected into this mixture and the temperature was increased to 275 °C. By thermolysis hot HDA can liberate Zn from Et_2Zn,[13] which facilitates the incorporation of Zn in the nanocrystals. After 30 min, the nanoparticles were isolated, washed and redispersed in hexane. Based on this generalized procedure, a series of hydrophobic Zn-SPIO nanoparticles of the general formula $Zn_xFe_{1-x}O{\cdot}Fe_2O_3$ ($x = 0$, 0.14, 0.26, 0.34, 0.76) were synthesized. The as-synthesized nanoparticles are uniform in size distribution (Table 1) as shown by transmission electron microscopy (TEM) (see ESI†). The final Zn-SPIO compositions were determined by atomic absorption spectroscopy and also characterized by X-ray powder diffraction (XRD, see ESI†). It should be noted that the standard XRD patterns

Table 1 Magnetic properties of $Zn_xFe_{1-x}O{\cdot}Fe_2O_3$ SPIOs

SPIO	Diameter/nm	Zn (x)	σ/emu g^{-1}	χ_o/cgs g^{-1}
1	4.6 ± 0.7	0	19.8	0.004
2	4.5 ± 0.8	0.14	26.8	0.010
3	4.5 ± 0.7	0.26	43.1	0.020
4	4.9 ± 0.7	0.34	54.1	0.025
5	4.5 ± 0.8	0.76	30.0	0.008

[a] *Harold C. Simmons Comprehensive Cancer Center, University of Texas Southwestern Medical Center at Dallas, 5323 Harry Hines Blvd, Dallas, TX 75390, USA. E-mail: Jinming.Gao@UTSouthwestern.edu; Fax: +1 214 645 6349; Tel: +1 214 645 6370*
[b] *Department of Physics, University of Texas at Arlington, 502 Yates Street, Arlington, TX 76019, USA*

† Electronic supplementary information (ESI) available: A typical experimental procedure for synthesizing Zn-SPIO nanoparticles and further characterization and measurements of Zn-SPIO nanoparticles and SPIO-micelles. See DOI: 10.1039/b801041b

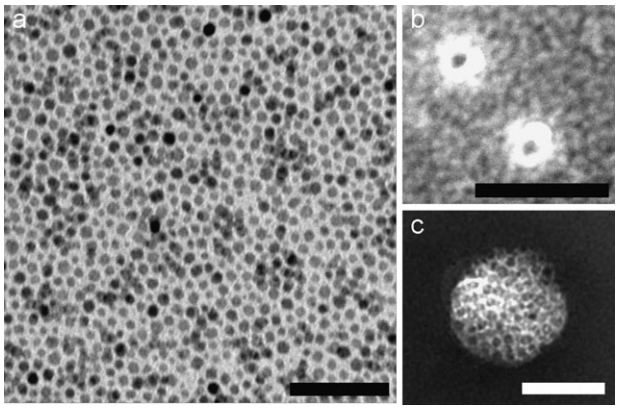

Fig. 1 TEM images of $Zn_xFe_{1-x}O{\cdot}Fe_2O_3$ ($x = 0.34$) (a) as synthesized hydrophobic nanoparticles; dark field TEM of (b) single DSPE-PEG and (c) clustered PEG-PLA micelles (scale bar = 50 nm).

for maghemite (γ-Fe_2O_3), magnetite, zinc ferrite and zinc-doped ferrites are nearly identical.[9]

Magnetization properties of the Zn-SPIO nanoparticles were measured using an alternating gradient magnetometer (AGM) at room temperature. The magnetization (σ) at 1.3 T increased from 19.8 emu g^{-1} for Fe_3O_4 to 54.1 emu g^{-1} for $x = 0.34$ Zn substitution, then decreased to 30 emu g^{-1} when $x = 0.76$ (Table 1). Studies on bulk materials indicate that when $x < 0.5$, replacement of Fe^{3+} (in the Fe_3O_4 lattice) by Zn^{2+} (from $ZnFe_2O_4$) at the A sites will cause a redistribution of Fe^{3+} at the A and B sites. This will result in an increased net magnetic moment due to the reduced antiferromagnetic interaction between the Fe^{3+} ions at A and B sites. On the other hand, when $x > 0.5$, further addition of $ZnFe_2O_4$ into the Fe_3O_4 lattice will lead to significantly increased B–B antiferromagnetic interactions, which decreases the net magnetic moment, eventually approaching zero as in pure $ZnFe_2O_4$.[9] Results from this study (Table 1) agree with the above trend.

These as-synthesized nanoparticles (Fig. 1a) are water insoluble due to the hydrophobic oleyl group on the nanoparticle surface. Previously, our group reported the encapsulation of magnetite nanoparticles in polymeric micelles with hydrophilic coatings.[14] 1,2-Distearoyl-*sn*-glycero-3-phosphoethanolamine-*N*-[methoxy(polyethylene glycol)] (DSPE-PEG, PEG MW = 5 kD) and poly(ethylene glycol)-block-poly(D,L-lactide) (PEG-PLA, PEG and PLA MW = 5 kD) were used as amphiphilic polymers for the encapsulation of Zn-SPIO nanoparticles. TEM images indicate that the DSPE-PEG copolymer (weight ratio to SPIO = 20 : 1) allowed the encapsulation of a single SPIO nanoparticle within each micelle (Fig. 1b) while the PEG-PLA copolymer (weight ratio to SPIO = 1 : 1) with a longer hydrophobic PLA segment led to encapsulation of a cluster of SPIO nanoparticles per micelle core (Fig. 1c).

The hydrodynamic diameters (D_H) of Zn-SPIO-loaded DSPE-PEG and PEG-PLA micelles were measured by dynamic light scattering (Table 2). T_1 and T_2 relaxation times were measured at 0.55 T (23.4 MHz) on a Resonance Maran Ultra scanner at 37 °C (Oxford Instruments, T_1: INVREC pulse sequence with TE = 5 × T_1; T_2: Carr–Purcell–Meiboom–Gill pulse sequence). T_1 and T_2 relaxivities (r_1 and r_2, respectively; see Table 2) were determined from the slope of the relaxation rates as a function of total metal concentration. Consistent with our magnetization data, Zn-SPIO with $x = 0.34$ exhibits the highest relaxivity value of 34.7 and 232.1 M $mM^{-1}s^{-1}$ for singly and clustered micelles, respectively. The r_2 values increase systematically, representing an approximately 3- and 6-fold enhancement for the DSPE-PEG (from 9.5 to 34.7 M mM^{-1} s^{-1}) and PEG-PLA (from 39.1 to 232.1 M $mM^{-1}s^{-1}$) systems, respectively. The short distance between the clustered SPIO nanoparticles inside the PEG-PLA core may permit magnetic coupling between the nanoparticles leading to a synergistic increase in r_2.[14,15] As a comparison, clinically approved Feridex® yielded r_1 and r_2 values (0.55 T) of 19.2 and 121.6 Fe mM^{-1} s^{-1} under identical experimental conditions. It is worth noting that the hydrodynamic diameter of a Feridex® sample is 80–150 nm,[16] significantly larger than the current PEG-PLA micelles.

To further evaluate the sensitivity of detection of Zn-SPIO agents, we obtained T_2-weighted images on a 4.7 T Varian INOVA scanner (spin-echo sequence, TR = 6000 ms, TE = 90 ms, room temperature). Fig. 2 compares MR intensity of Zn-SPIO ($x = 0.34$)-loaded PEG-PLA micelles with that of Feridex® at the same metal concentration. For quantitative comparisons, we defined sensitivity as the micelle concentration at which the MRI signal intensity decreases to 50% of that for pure water in T_2-weighted images.[14] The Zn-SPIO ($x = 0.34$)-loaded PEG-PLA micelles yield a detection limit of 0.8 μg mL^{-1} compared to 2.1 μg mL^{-1} for Feridex® (see ESI†).

In summary, through careful systematic study we have demonstrated a mixed spinel strategy to increase the magnetization of SPIOs, which in turn increases the T_2 relaxivity and improves the sensitivity of detection by MRI. This strategy exploits the complex magnetic behavior resulting from the

Table 2 Micelle size and relaxivity values for different formulations

SPIO	Micelle formulation	Micelle size/nm	r_1/M mM^{-1} s^{-1}	r_2/M mM^{-1} s^{-1}	r_2/r_1
1	DSPE-PEG	16.0 ± 1.0	2.5 ± 0.3	9.5 ± 0.9	3.8
2	DSPE-PEG	19.8 ± 1.3	5.0 ± 0.5	14.5 ± 0.9	2.9
3	DSPE-PEG	15.9 ± 0.4	7.5 ± 0.9	22.4 ± 2.8	3.0
4	DSPE-PEG	18.2 ± 2.2	11.3 ± 2.5	34.7 ± 1.5	3.1
5	DSPE-PEG	15.3 ± 1.6	2.4 ± 0.2	7.4 ± 0.5	3.1
1	PEG-PLA	62.8 ± 9.9	1.8 ± 0.6	39.1 ± 11.6	22.2
2	PEG-PLA	67.2 ± 7.3	1.0 ± 0.2	75.7 ± 14.1	73.2
3	PEG-PLA	63.6 ± 7.7	3.5 ± 0.4	193.1 ± 23.3	55.7
4	PEG-PLA	68.0 ± 2.9	6.8 ± 0.9	232.1 ± 37.6	34.0
5	PEG-PLA	57.0 ± 8.6	1.4 ± 0.5	64.1 ± 4.0	45.9

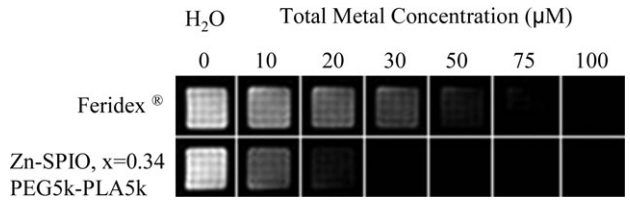

Fig. 2 T_2-weighted MRI image (4.7 T, spin-echo sequence: TR = 6000 ms, TE = 90 ms).

magnetic disorder in the crystal lattice caused by the inclusion of non-magnetic normal spinel $ZnFe_2O_4$ in an inverse spinel ferrite. With comparable FDA RDI values for Zn and Fe, toxicity of Zn would not be a major biocompatibility concern. The availability of these novel Zn-SPIO nanoparticles will allow for the development of ultrasensitive MR probes for molecular imaging applications, while providing a well controlled system for fundamental studies of the correlation of magnetic properties of ferrites with their MR relaxivities in water.

This work was supported by a NIBIB grant (R21-EB005394) to JG. CB is grateful for the support of a NIBIB minority supplement grant. CK thanks DOD for a Breast Cancer Research Program Multidisciplinary Postdoctoral Award (W81XWH-06-1-0751). This is report CSCN31 in the Cell Stress and Cancer Nanomedicine Program at UTSW.

Notes and references

1 Y. X. J. Wang, S. M. Hussain and G. P. Krestin, *Eur. Radiol.*, 2001, **11**, 2319.
2 J. W. M. Bulte and D. L. Kraitchman, *NMR Biomed.*, 2004, **17**, 484.
3 D. L. J. Thorek, A. K. Chen, J. Czupryna and A. Tsourkas, *Ann. Biomed. Eng.*, 2006, **34**, 23.
4 J. Wan, W. Cai, X. Meng and E. Liu, *Chem. Commun.*, 2007, 5004.
5 J. H. Lee, Y. M. Huh, Y. W. Jun, J. W. Seo, J. T. Jang, H. T. Song, S. Kim, E. J. Cho, H. G. Yoon, J. S. Suh and J. Cheon, *Nat. Med.*, 2007, **13**, 95.
6 R. A. McCurrie, *Ferromagnetic Materials: Structure and Properties*, Academic Press, New York, 1994.
7 J. E. Thompson, *The Magnetic Properties of Materials*, Stonebridge Press, Bristol, 1968.
8 E. W. Gorter, *Nature*, 1950, **165**, 798.
9 P. A. Dickof, P. J. Schurer and A. H. Morrish, *Phys. Rev. B: Condens. Matter Mater. Phys.*, 1980, **22**, 115.
10 J. F. Hochepied, P. Bonville and M. P. Pileni, *J. Phys. Chem. B*, 2000, **104**, 905.
11 S. B. Goldhaber, *Regul. Toxicol. Pharmacol.*, 2003, **38**, 232.
12 S. Sun and H. Zeng, *J. Am. Chem. Soc.*, 2002, **124**, 8204.
13 J. Hambrock, M. K. Schroeter, A. Birkner, C. Woell and R. A. Fischer, *Chem. Mater.*, 2003, **15**, 4217.
14 H. Ai, C. Flask, B. Weinberg, X. Shuai, M. D. Pagel, D. Ferrel, J. Duerk and J. Gao, *Adv. Mater.*, 2005, **17**, 1949.
15 V. Russier, C. Petit and M. P. Pileni, *J. Appl. Phys.*, 2003, **93**, 10001.
16 R. Weissleder, D. D. Stark, B. L. Engelstad, B. R. Bacon, C. C. Compton, D. L. White, P. Jacobs and J. Lewis, *AJR, Am. J. Roentgenol.*, 1989, **152**, 167.